Miner Deposita (2012) 47:411–424
DOI 10.1007/s00126-011-0374-3

ARTICLE

Talc mineralisation associated with soft hematite ore, Gongo Soco deposit, Minas Gerais, Brazil: petrography, mineral chemistry and boron-isotope composition of tourmaline

Alexandre Raphael Cabral · Michael Wiedenbeck · Francisco Javier Rios · Antônio Augusto Seabra Gomes Jr · Orlando Garcia Rocha Filho · Richard David Jones

Received: 31 August 2010 / Accepted: 27 June 2011 / Published online: 30 July 2011

Abstract Talc mineralisation occurs as hematite–talc schist between soft hematite ore and dolomitic itabirite at Gongo Soco, Quadrilátero Ferrífero of Minas Gerais, Brazil. The hematite–talc schist and soft hematite have a prominent tectonic foliation of tabular hematite. Tabular hematite without preferential orientation is superimposed on the tectonic foliation. The talcose schist is enriched in F and has a constant Fe/S ratio. Electron-microprobe analyses indicate trace amounts of S in different generations of hematite. The whole-rock Fe/S ratio possibly represents sulfate S from hematite-hosted fluid inclusions. Fluid inclusions in foliation-overprinting hematite and chlorite geothermometry from talcose rocks suggest, respectively, temperatures from <200°C to ~300°C. Tourmaline, a rarely observed mineral in the hematite–talc schist, belongs to the alkali group and falls in the dravite compositional field. Boron-isotope determinations of tourmaline crystals, using secondary ion mass spectrometry, vary from −20‰ to −12‰ $\delta^{11}B$. This compositional isotopic range and the tourmaline chemical composition suggest a meta-evaporitic origin. A non-marine evaporitic setting is the most likely source of acidic, highly oxidising fluids, which resulted in the abundant F-bearing talc and the presence of otherwise immobile Ti in hematite. Oxidising brines were channelled along shear zones and converted dolomitic itabirite into the Gongo Soco soft hematite and the talc mineralisation. The latter is envisaged as the hydrothermal wall-rock alteration of dolomitic itabirite, which gave rise to the soft hematite ore.

Keywords Talc · Hematite · Mineral chemistry · SIMS · Boron isotopes · Gongo Soco · Quadrilátero Ferrífero · Minas Gerais · Brazil

Editorial handling: R. Perez Xavier

Electronic supplementary material The online version of this article (doi:10.1007/s00126-011-0374-3) contains supplementary material, which is available to authorized users.

A. R. Cabral (✉)
Exploration Geology, Rhodes University,
PO Box 94, Grahamstown 6140, South Africa
e-mail: alexandre.cabral@tu-clausthal.de

M. Wiedenbeck
Helmholtz-Zentrum Potsdam, Deutsches GeoForschungsZentrum,
Telegrafenberg C128,
14473, Potsdam, Germany

F. J. Rios
Centro de Desenvolvimento da Tecnologia Nuclear
(CDTN/CNEN),
30123-970, Belo Horizonte-MG, Brazil

A. A. Seabra Gomes Jr
Gerência de Exploração Mineral de Ferrosos (GAEMF), Centro Tecnológico de Ferrosos–Miguelão, VALE, Fazenda Rio do Peixe,
Galpão de Testemunhos,
34000-000, Nova Lima-MG, Brazil

O. G. Rocha Filho
Rua Ceará, 1338/701,
30150-311, Belo Horizonte-MG, Brazil

R. D. Jones
1636 East Skyline Drive,
Tucson, AZ 85178, USA

Present Address:
A. R. Cabral
Technische Universität Clausthal, Lagerstätten und Rohstoffe,
Adolph-Roemer-Str. 2A,
38678, Clausthal-Zellerfeld, Germany

Introduction

The supergene leaching of gangue minerals such as carbonate and quartz from banded Fe-rich rocks (i.e.

banded iron formations) is commonly regarded as an important hematite ore-forming process. In the world-class Quadrilátero Ferrífero of Minas Gerais, Brazil, the weathering-induced removal of gangue minerals has been considered by many authors to have transformed itabirite into hematite ore (e.g. Dorr 1964; Eichler 1967; Spier et al. 2003). This concept has been challenged by a few authors (e.g. Guimarães 1953; Cabral et al. 2003), who propose that soft hematite ore could be formed via a hydrothermal mechanism. Such a hydrothermal model, requiring the removal of gangue minerals by hydrothermal fluids, would predict the formation of Mg-rich minerals, such as talc, in the wall rocks (e.g. Dalstra and Guedes 2004). The Gongo Soco mine in Minas Gerais is a soft hematite deposit in which hydrothermal alteration is expressed as talc mineralisation spatially associated with soft hematite ore. Here, the Gongo Soco talc mineralisation is described, and the origin of the hydrothermal fluids is constrained by the B-isotope signature of tourmaline.

Analytical methods

Electron-microprobe analyses were carried out with a Cameca SX100, at the Laboratoire de Microanalyse, Université Laval, Quebec, Canada, on talc and hematite, and at the Technische Universität Clausthal, Germany, on carbonate, chlorite and tourmaline. All elements had their $K\alpha$ X-ray emission lines measured (Tables 1, 2, 3, 4 and 5 in the Electronic Supplementary Material section). Backscattered-electron imaging was conducted with a Tescan-Vega-LMU scanning electron microscope, equipped with an Oxford Instruments IncaPentaFETx3 energy-dispersive detector at Rhodes University, South Africa.

Whole-rock chemical analyses were performed at Activation Laboratories Ltd., Ancaster, Ontario, Canada, using a variety of analytical techniques. Elements determined by instrumental neutron activation analysis, total digestion inductively coupled plasma technique and ICP mass spectrometry are specified in Table 6. Other techniques applied were ion selective electrode for F, prompt gamma neutron activation analysis (PGNAA) for B, and cold vapour–flow injection mercury system for Hg.

Hematite-hosted fluid inclusions were studied at the Centro de Desenvolvimento de Tecnologia Nuclear, Belo Horizonte, Brazil, using a Leica DMR-XP and a Olympus BX51 infrared microscope. The Leica microscope is equipped with a 100-W transmitted-light illuminator with halogen-light bulbs as a source of visible and very-near-infrared radiation. Doubly polished sections of about 50- to 80-mm thick were prepared. Hematite crystals generally exhibited good transparency in the very-near-infrared spectrum. A Q-Imaging Quicam Fast 1394 very-near-infrared camera and an Eletrophysics Microniewer Model 7290-A IR camera, both coupled to a HP high-resolution monitor, provided infrared images (Rosière and Rios 2006). For the observation of thicker hematite sections, where the transparency under the regular halogen lamp was unsatisfactory, an infrared emission regulator with a 50-W/12-V Hosobuchi iodine-tungsten lamp was used. The infrared beam between the lamp bulb and the sample covered an overall distance of 40 cm. A maximum voltage of 5 V was applied during the measurements in order to avoid overheating of the sample.

Secondary ion mass spectrometry

Boron-isotope analyses were obtained using the Cameca ims 6f secondary ion mass spectrometry (SIMS) instrument in Potsdam, Germany. Prior to analyses the 25.4-mm diameter round polished thin sections were ultrasonically cleaned for 5 min in high purity ethanol and were coated with a 35-nm-thick film of high-purity gold. Samples were stored for several days in a high-vacuum sample chamber (Wiedenbeck et al. 2004) in advance of the actual measurement session. The total pressure in the secondary ion source was of the order 5 e^{-8} Pa at the time of analysis.

SIMS measurements employed a nominally 12.5-kV, 800-pA $^{16}O^-$ primary beam, which was focussed to about 8-μm diameter at the sample surface. Secondary ions were extracted using a 10.0-kV potential. We operated the mass spectrometer at a mass resolving power of M/dM=1200, sufficient to resolve the $^{11}B^+$ mass station from the nearby $^1H^{10}B^+$ peak, in conjunction with a 50-V-wide energy window to which no offset voltage was applied. A single cycle of our peak stepping sequence consisted of 9.95 Da (0.1 s per cycle, used for magnet settling and during the automatic presputtering), ^{10}B (2 s) and ^{11}B (1 s); a full analysis consisted of 100 cycles. Each analysis was preceded by a 180-s preburn in order to remove the gold coat and to establish equilibrium sputtering conditions at the point of analysis, and hence a complete analysis had a duration of 9 min. A typical measurement had an uncertainty of around 0.3‰ to 0.4‰ (1 s), which is only marginally worse than that predicted by ion counting statistics.

We calibrated the instrumental mass fractionation (IMF) using a suite of four natural tourmaline reference materials (RM) for which boron isotopic compositions had been determined by wet chemistry. These included the single crystal elbaite, dravite and schorl materials described by Dyar et al. (2001), and the B4 multi-grain material described by Gonfiantini et al. (2003) and Tonarini et al. (2003). The repeatability on single materials was between 0.7‰ and 1.5‰ (1 s) and the overall reproducibility of the entire pool of calibration measurements (n=32) was ±1.6‰. As in

previous tourmaline studies, we tended to find that the elbaite RM yielded a 1‰ to 2‰ larger IMF (i.e., tended to measure low $^{11}B^{+}/^{10}B^{+}$ ratios) than would be predicted based on the reference values published by Leeman and Tonarini (2001). As this offset is roughly comparable to the overall uncertainty of our analytical method, we are unable to conclude that such a difference can be seen as evidence for the presence of a significant chemical matrix effect. Based on the above observations, we believe that the SIMS B-isotope results reported here are robust to roughly $a\pm$ 1.5‰ (1 s) level.

Geological setting

Gongo Soco is one of numerous iron-ore deposits of the Quadrilátero Ferrífero (Fig. 1). The Quadrilátero Ferrífero is situated in the southernmost part of the São Francisco craton, which is delimited by orogenic belts of Brasiliano age, i.e. ~0.6 Ga (Alkmim and Marshak 1998, and references therein). There are three major geological domains in the Quadrilátero Ferrífero: (1) Archaean to Proterozoic granitic–gneissic terrains; (2) the greenstone-belt succession of the Rio das Velhas Supergroup, on which (3) the metasedimentary sequence of the Minas Supergroup unconformably rests.

The basal sequence of the Minas Supergroup is the Caraça Group, which is divided into the Moeda and Batatal formations (Fig. 2). The Moeda Formation comprises quartzite and metaconglomerate, including Witwatersrand-like metaconglomerate (e.g. Koglin et al. 2010). It is overlain by metapelitic rocks of the Batatal Formation, which is transitional to an overlying itabirite unit, the Itabira iron formation of Harder and Chamberlin (1915), later designated as the Itabira Group (Dorr 1969). The Itabira Group consists of two formations: the Cauê Itabirite (also known as Cauê Formation), a metamorphosed, laminated iron formation, i.e. itabirite, which grades

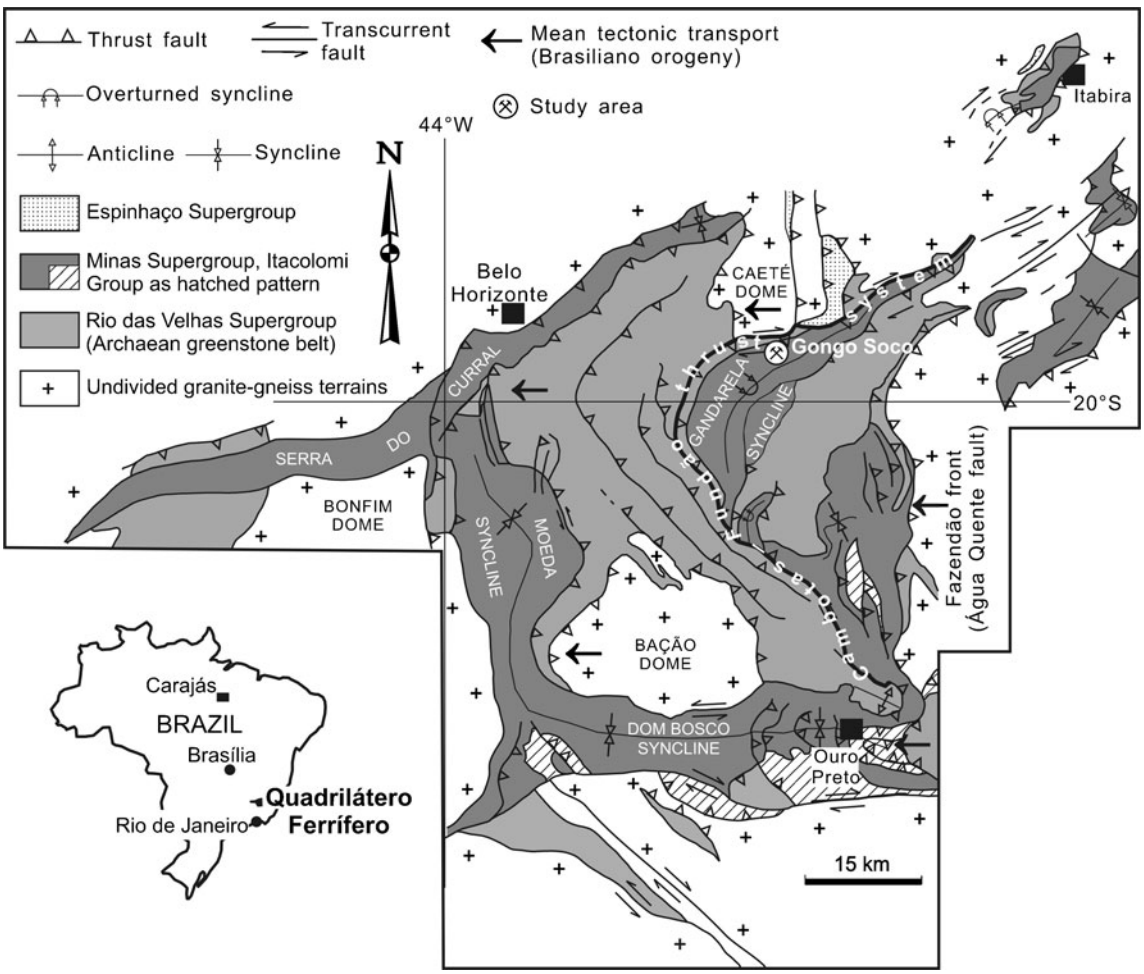

Fig. 1 Simplified geological map of the Quadrilátero Ferrífero (modified after Dorr 1969 and Rosière et al. 2008), with the location of the study area, Gongo Soco

Fig. 2 Schematic lithostratigraphic column emphasising the Caraça and Itabira groups of the Minas Supergroup (adapted from Harder and Chamberlin 1915; Dorr 1969; Alkmim and Marshak 1998)

upwards into dolomitic rocks of the Gandarela Formation. The Cauê Formation hosts the economically important iron-ore deposits of the Quadrilátero Ferrífero. The age of the Cauê Formation is constrained between 2.58 and 2.42 Ga (Hartmann et al., 2006). Unconformably superjacent to the Itabira Group is the Piracicaba Group, the upper clastic sequence of the Minas Supergroup.

The dome-and-keel architecture of the Quadrilátero Ferrífero (Fig. 1) is thought to result from the emplacement of basement domes against the Rio das Velhas and Minas strata during the collapse of the Transamazonian orogeny (e.g. Alkmim and Marshak 1998). West-vergent thrust faults overprint the dome-and-keel architecture, leading to tectonic stacking of the Rio das Velhas and Minas supergroups. This overprint on structures related to the ~2.0-Ga Transamazonian orogeny is attributed to the ~0.6-Ga Brasiliano orogeny (e.g. Alkmim and Marshak 1998; Hippertt and Davis 2000; Rosière and Rios 2004; vide Rosière et al. 2008, for a discussion). One of such structures is the Cambotas–Fundão thrust system (Fig. 1). The Brasiliano overprint produced penetrative tectonic fabrics in the supracrustal rocks of the Minas Supergroup in the central and eastern parts of the Quadrilátero Ferrífero. In hematite-bearing rocks, i.e. itabirite and associated hematite ore, the Brasiliano overprint resulted in a schistose hematite fabric. The eastward overprint of pre-existing structures by Brasiliano tectonic fabrics broadly coincides with regional metamorphic grades, which increase eastward from lower greenschist to lower amphibolite facies (Herz 1978; Pires 1995). No plutonic rocks of Brasiliano age are known in the Quadrilátero Ferrífero, but the Brasiliano event produced an eastward isotopic resetting of older magmatic rocks (e.g. Noce 2000).

Gongo Soco hematite deposit

Gongo Soco is a high-grade soft hematite deposit, currently being mined by Companhia Vale do Rio Doce (VALE). Soft hematite refers to pulverulent ore. The host rock to the Gongo Soco soft hematite is itabirite of the Cauê Formation, which is between 300 and 400 m thick. The soft hematite orebody is about 1,300 m long and trends E–W (Fig. 3). This direction is slightly discordant to the ~070°-trending host itabirite. The soft hematite orebody is delimited by E–W-striking, S-dipping shear zones.

The soft hematite ore has an average Fe content of ~67%. Compared with other iron-ore deposits in the Quadrilátero Ferrífero, Gongo Soco is characterised by relatively high contents of Mn. This manganiferous soft hematite, locally known as 'pulverulent hematite ore', has ~64% Fe and ~1% Mn. Both soft ore varieties, hereafter jointly referred to as soft hematite, show a prominent tectonic foliation, which is given by the planar arrangement of tabular hematite (Cabral et al. 2003).

Similar to the soft hematite ore, the host itabirite at Gongo Soco displays a penetrative tectonic foliation defined by tabular hematite. Submillimetric layers of tabular hematite constitute dark-coloured bands that alternate with light-coloured bands of gangue minerals. The latter are dominated by quartz and subordinate amounts of carbonate, talc, chlorite and white mica. The silicate minerals are aligned parallel to the foliation-forming tabular hematite. Talc is found in pressure-shadow domains on porphyroblasts of hematite pseudomorphs after magnetite, i.e. martite (Fig. 4a). Carbonate is partially replaced by talc, with or without intergrowth of chlorite (Fig. 4b). The carbonate mineral is dolomite, which has a compositional

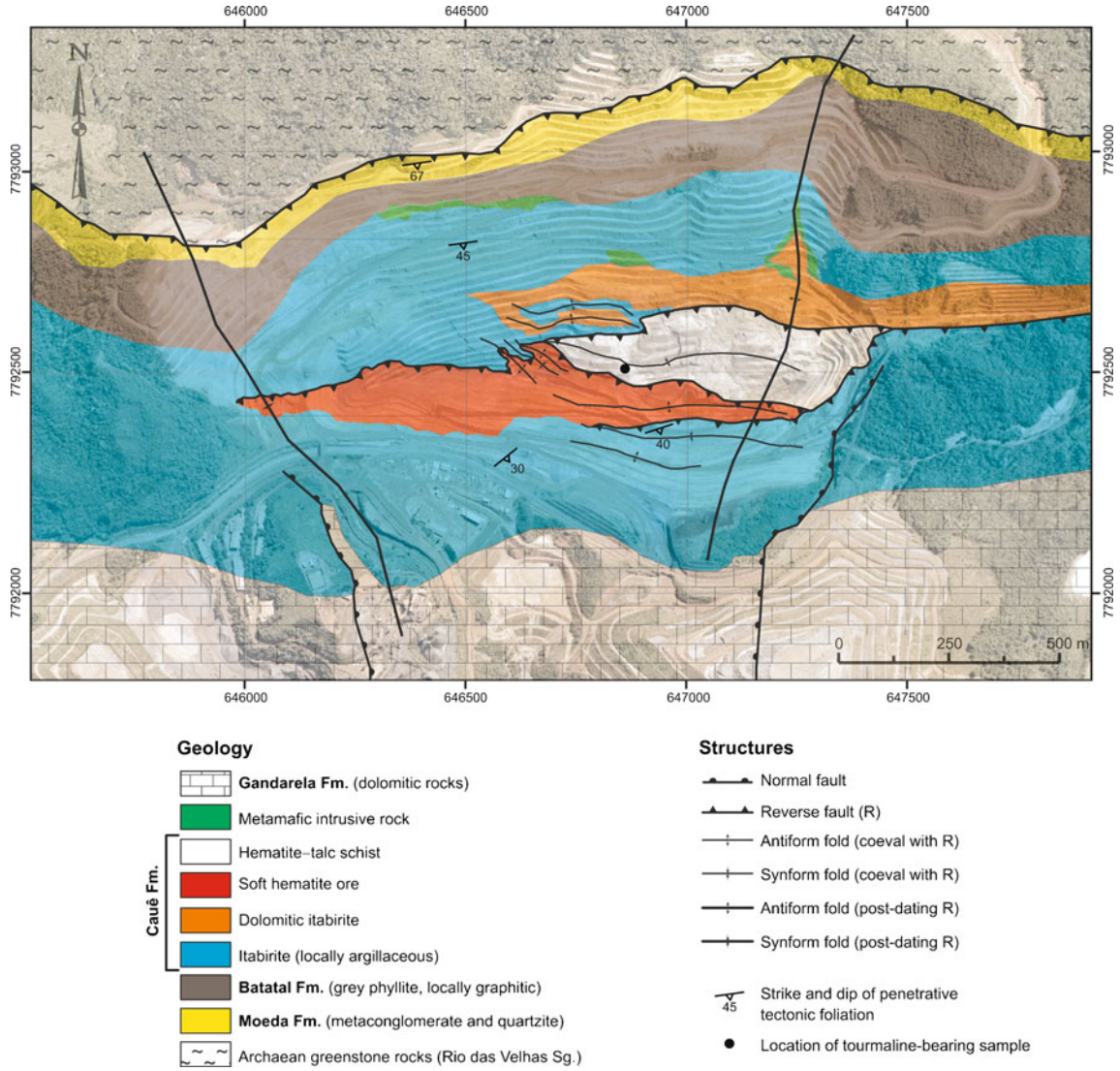

Fig. 3 Simplified map of the Gongo Soco open cast; geology by Orlando G. Rocha Filho and Antônio A. Seabra Gomes Jr. Deepening of the open cast has exposed dolomite pods within the talc mineralisation (not indicated in the map)

range from Mn-poor dolomite to Mn-rich ankerite. Its MnO content varies from ~0.6 wt% in dolomite to ~10 wt% in ankerite (Table 1 ESM). Aggregates of chlorite-forming foliation are enriched in Mg, with Fe/(Fe+Mg) ratios of about 0.25 (Table 2 ESM). The presence of chlorite and white mica is consistent with metamorphic conditions of greenschist facies.

Talc mineralisation

Early resource evaluations indicated ~12 Mt of talc ore suitable for metallurgical applications as fluxing material (O. G. Rocha Filho, 1999, private company report, Socoimex). The talc mineralisation occurs as tightly folded hematite–talc schist between the soft hematite orebody and the wall-rock itabirite (Figs. 3 and 5). Part of the wall-rock itabirite in contact with the hematite–talc schist is dolomitic itabirite (Fig. 3). The talcose rock is characterised by the penetrative tectonic foliation observed in the soft hematite orebody. The contacts of the talc-rich schist with the wall rocks are shear zones that are generally subparallel to those delimiting the soft hematite orebody. The shear zones are reverse faults, which are related to the Cambotas–Fundão thrust system (Fig. 1) of Brasiliano age (e.g. Rosière and Rios 2006).

Locally, the contacts between the hematite–talc schist and wall rocks are overprinted by disseminations and pockets of chaotically oriented crystals of specular hematite and plumose-like aggregates of talc. Quartz, if any, occurs in hematite-rich pockets that may host palladiferous gold mineralisation. This auriferous mineralisation made Gongo

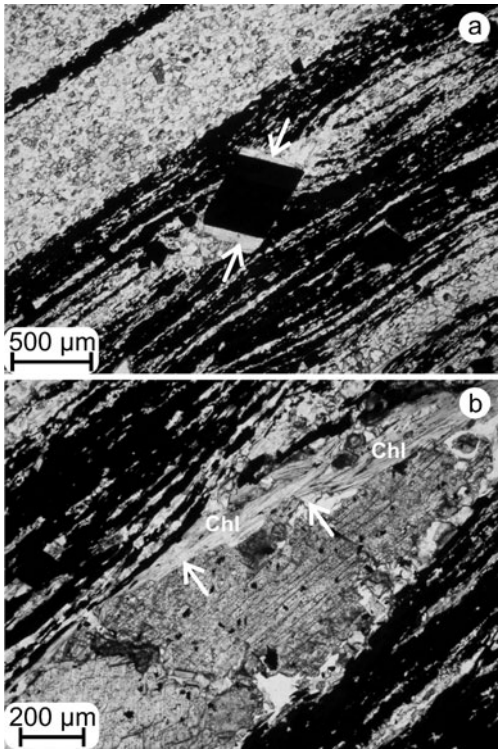

Fig. 4 Transmitted-light photomicrographs of fresh wall-rock itabirite. Submillimetric black layers of tabular hematite alternating with quartz-rich bands (*colourless*). Opaque crystals with lozenge-like shapes are porphyroblasts of hematite after magnetite, i.e. martite. **a** Porphyroblast of martite (*centre*) with talc in pressure-shadow domains (*arrows*). **b** Carbonate domain is shown in the centre (higher relief, *cloudy* appearance) and comprises dolomite and ankerite (indistinguishable in the picture). The carbonate domain is partially replaced by talc (*arrows*) and chlorite (*Chl*)

Soco a famous underground gold mine in the nineteenth century (e.g. Henwood 1871; Cabral 2006). Gongo Soco belongs to the platiniferous Au–Pd belt of Minas Gerais (Cabral et al. 2009).

Fig. 5 Contact between hematite–talc schist (*white*) and soft hematite ore. Orlando G. Rocha Filho (*left*) and Richard D. Jones pose as scales

Open-cast mining for iron ore has recently reached depths that have exposed dolomite pods surrounded by dolomite-bearing hematite–talc schist within the otherwise dolomite-free talcose schist.

Petrography and mineral chemistry

The hematite–talc schist is composed of alternating talcose and hematitic bands, which resemble those of the fresh wall-rock itabirite. These bands define a compositional layering, here referred to as 'S_0'. The earliest recognisable fabric in the S_0 layers is granoblastic hematite, hereafter called 'S_0 hematite'. The S_0 hematite is overprinted by a penetrative foliation, labelled as 'S_1', of tabular hematite, the 'S_1 hematite' (Fig. 6a). The S_1 hematite occurs as schistosity in shear zones and as axial planar foliation at fold hinges. At fold hinges, the S_0 layers have spaced shear bands of local S_1 hematite, which is truncated by the penetrative axial planar S_1 hematite (Fig. 6a, b). The S_1-forming talc is locally cross-cut by veinlets that contain radial to plumose-like aggregates of tabular hematite (Fig. 6c, d). Talc also manifests itself as infill in sets of microfractures that truncate S_0 layers. Tourmaline is occasionally spotted within the talcose matrix (Fig. 6e).

The S_1 fabrics are obliterated by mineral disseminations. These disseminations are frequently observed at the contacts between hematite–talc schist and soft hematite ore. The disseminations consist of tabular hematite, talc and minor chlorite. This tabular hematite is here referred to as 'S_1-overprinting hematite'. The S_1-overprinting hematite locally forms concentrations of randomly oriented crystals. Their concentrations occur immediately adjacent to talcose domains (Fig. 6f). In the talcose domains, the S_1-overprinting hematite is sparsely interspersed with talc and minor chlorite. The latter, identified as 'S_1-overprinting talc and chlorite', have no preferred orientation. The S_1-overprinting chlorite is more enriched in Mg, with Fe/(Fe+Mg) ratios between 0.13 and 0.15 (Table 2 ESM), than that dispersed in the fresh wall-rock itabirite.

The S_1-overprinting hematite and associated talc and chlorite can be recognised in the field by a finger-staining, Mn-bearing soft material (wad) of black to dark brown colour. The manganiferous material is interstitial. Figure 7a shows aggregates of tabular hematite and chlorite within a groundmass of Mn-bearing material (Fig. 7b), which contains Al (Fig. 7c) and Cl (Fig. 7d). Qualitative micro-analyses using EDS have suggested that C is a major component, pointing to a carbonaceous wad containing minor amounts of Al and Cl.

Fluorine, in contents of up to ~0.5 wt%, is present in both S_1-forming talc and non-oriented, S_1-overprinting talc (Table 3 ESM). The talc has some Fe (2.1–3.2 wt% FeO) and Al (0.1–1.4 wt% Al_2O_3). There are no obvious

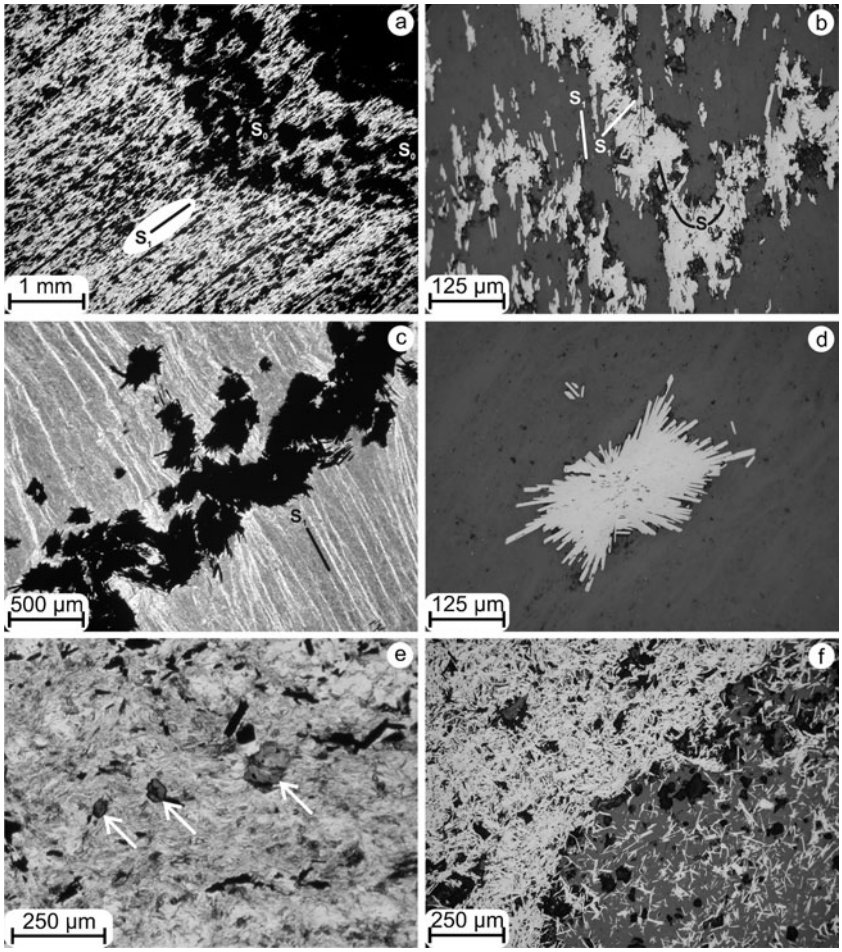

Fig. 6 Photomicrographs in transmitted and reflected light, respectively left and right columns, of hematite–talc schist. In the *left* column, hematite appears *black*, whereas talc is *colourless*. In the *right* column, hematite is *white*, whereas talc appears in shades of *grey*. **a** Penetrative axial planar foliation (S_1) is given by talc and tabular hematite. They define a tectonic foliation, the S_1 foliation, which post-dates the compositional banding (S_0) at the fold hinge (*upper right corner*). **b** The fold-hinge zone comprises S_0 layers with spaced shear bands of local S_1 hematite, oblique to the penetrative S_1 hematite (*subvertical* in the photomicrograph). **c** A veinlet of tabular hematite truncates S_1-forming talc. **d** The veinlet hematite, as that shown in **c**, consists of radial, plumose-like aggregates. **e** Tourmaline crystals (*arrows*) within the hematite–talc schist. **f** Contact between hematite ore (*upper left*) and talcose rock (*lower right*). Tabular hematite (*white*), talc and chlorite (indistinguishable in shades of *grey*) are randomly oriented

differences in the mineral chemistry of the above-mentioned talc generations. Hematite, however, seems to record cryptic nuances in the contents of trace elements with respect to hematite generation. The highest values of Ti (3335 μg/g), Al (2451 μg/g) and S (114 μg/g) come from non-oriented, S_1-overprinting hematite, whereas their maximum values in S_1 hematite are considerably lower, i.e. 852 μg/g Ti, 742 μg/g Al and 60 μg/g S (Table 4 ESM).

Tourmaline is a rarely observed mineral in the hematite–talc schist. It occurs as sparsely dispersed crystals of up to ~150 μm in length within the talcose matrix (Fig. 6e). The tourmaline falls in the dravite compositional field, with Mg/(Mg+Fe) and X/(X+Na) ratios in the range from 0.63 to 0.77 and from 0.08 to 0.25, respectively, where X represents vacancies in the X site (Table 5 ESM). The tourmaline plots along the povondraite–"oxy-dravite" trend, cross-cutting the schorl–dravite tie line (Fig. 8).

Whole-rock chemistry

Samples of hematite–talc schist (without dolomite) have compositional ranges from 2.8 to 13.7 wt% Mg and from 6.3 to 43.0 wt% Fe (Table 6 ESM). Manganese contents vary from a few hundred micrograms per gram to 3.5 wt%. Fluorine is present in amounts extending from 0.05 to 1.0 wt% (Fig. 9a). The latter value coincides with the highest Ca content in dolomite-free samples of hematite–talc schist and suggests the existence of fluorite. Talc is the dominant F-bearing mineral and likely accounts for whole-rock samples of up to about 0.4 wt% F. These samples plot within the limits defined by the minimum and maximum contents of F, with their respective Mg values (Table 3 ESM), assuming the hypothetical case of whole-rock chemistry controlled by these talc compositions only. Sulfur values are low, from 0.01 to 0.04 wt%, but they are positively correlated with total Fe (Fig. 9b). Except for a single sample (6 μg/g), B abundances are below 2 μg/g, which is not detectable using the PGNAA method. Mercury can sporadically be found in contents as high as 782 ng/g.

One sample of dolomite-bearing hematite–talc schist, which forms a halo around a dolomite pod within the talc orebody, has 0.08 wt% F. The dolomite pod, however, contains no F above the detection limit of 0.01 wt%.

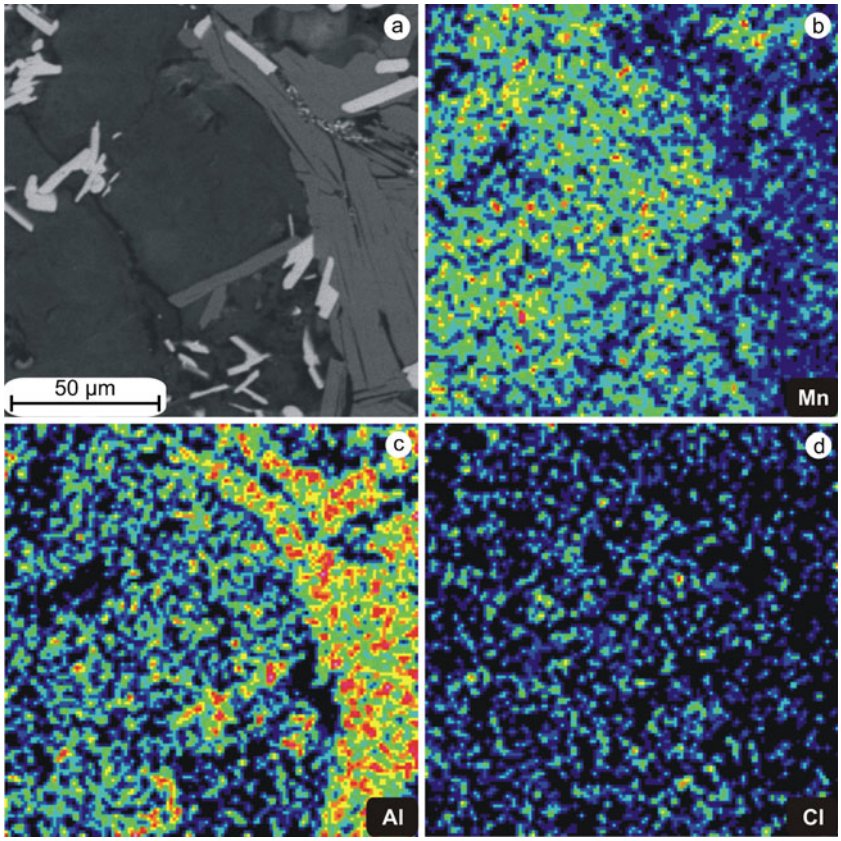

Fig. 7 **a** Backscattered-electron image of finger-staining wad (*dark grey*), which is interstitial to tabular hematite (*white*) and chlorite (*light grey*). Wad is found as *black* to *dark brown patches*, a few millimetres across, at the contacts between hematite–talc schist and soft hematite ore and in Mn-bearing portions of the soft hematite ore. X-ray maps for the same picture section as in **a** for **b** Mn, **c** Al and **d** Cl. Energy-dispersive microanalyses indicate that the wad material is carbonaceous

Petrography of hematite-hosted fluid inclusions

The S_1-overprinting hematite of Fig. 6f has provided the best material for fluid-inclusion petrography using infrared microscopy. The infrared microscopy has shown that the S_1-overprinting hematite consists of two types of hematite: (1) granular hematite, which occurs as remnants within (2) tabular hematite (Fig. 10a).

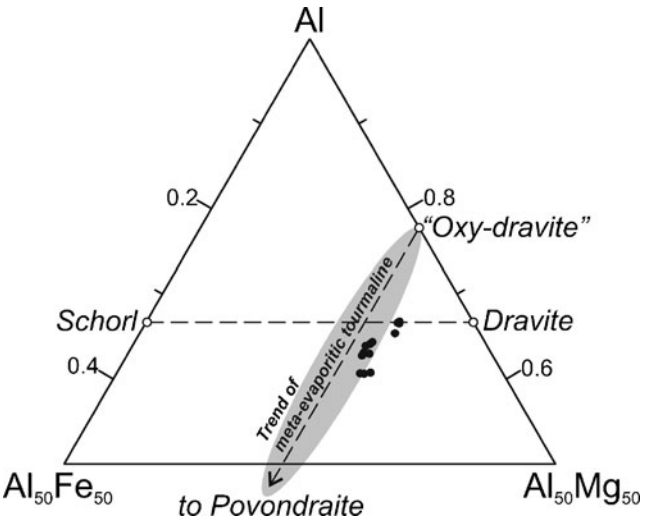

Fig. 8 *Upper* portion of an Al–Fe–Mg ternary diagram for tourmaline within the hematite–talc schist (Table 5 ESM). Meta-evaporitic tourmaline typically follows a trend along the join line between "oxy-dravite" and povondraite (Henry et al. 2008)

1. Rarely observed, the granular hematite lacks well formed crystal faces and hence differs from the granoblastic (S_0) hematite from more severely metamorphosed terrains of the Quadrilátero Ferrífero, where metamorphism produced well faceted granoblasts (e.g. Conceição iron-ore mine, Rosière and Rios 2004), and in the Espinhaço Supergroup (Lima et al. 2009). Fluid inclusions in the granular hematite tend to cluster in the core, whereas the margins are limpid, i.e. devoid of fluid inclusions (Fig. 10b). This fluid-inclusion arrangement indicates that the host hematite underwent incipient recrystallisation.
2. The tabular hematite can further be divided into two groups. An early group is represented by somewhat elongated crystals without arrays of cleavage-controlled fluid inclusions. In this regard, the fluid inclusions are randomly distributed (Fig. 10c) and resemble those of the granular hematite. These fluid inclusions are likely relics of the transition of granular into tabular hematite. A late group is given by well elongated laths that host arrays of cleavage-controlled fluid inclusions (Fig. 10d).

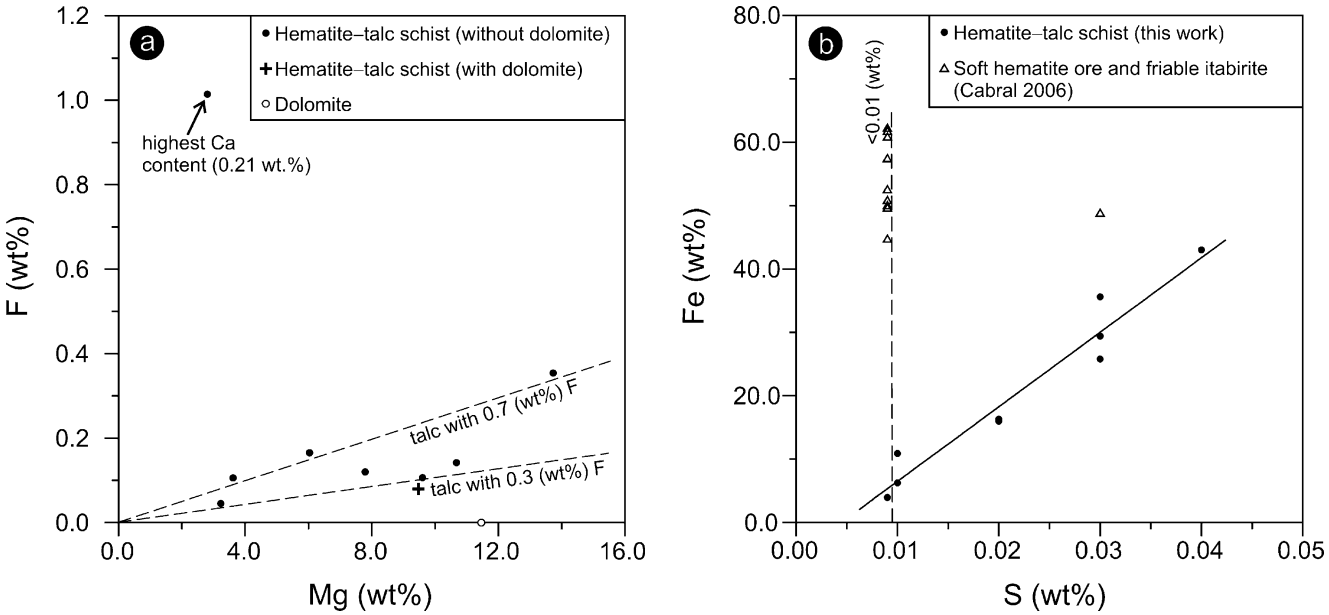

Fig. 9 **a** Diagram for whole-rock contents of Mg vs. F. Talc is the dominant F-bearing mineral and most samples plot within, or near, the limits defined by the dashed lines. These lines represent the minimum and maximum contents of F, with their respective Mg values, obtained by electron-microprobe analyses (Table 3 ESM), if the whole-rock chemistry is controlled by these talc compositions only. **b** Diagram for whole-rock contents of S vs. Fe. The elements show a strong positive correlation (regression line) in samples of hematite–talc schist. Other Fe-rich rocks from Gongo Soco, which were previously analysed using the same analytical techniques, are plotted for comparison (vide Discussion)

The fluid inclusions within the S_1-overprinting hematite are essentially aqueous and mostly monophasic. A few biphasic (liquid+vapour) fluid inclusions were found. The fluid inclusions were prohibitively small for detailed microthermometric studies. Only two measurements of homogenisation temperatures, between 140°C and 160°C, were obtained from biphasic fluid inclusions. These homogenisation temperatures and the predominance of

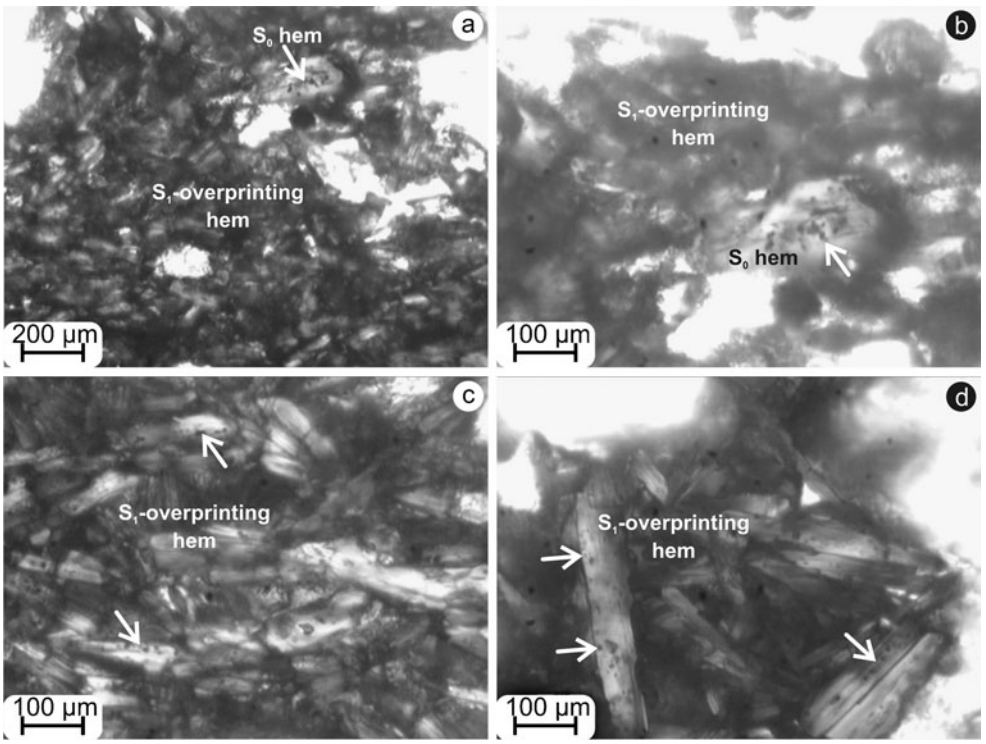

Fig. 10 Infrared photomicrographs; hematite appears in shades of *grey*. The sample comes from a contact between hematite–talc schist and soft hematite ore. **a** Chaotically oriented crystals of tabular hematite (S_1-overprinting hem, dark grey) with a remnant of granular hematite (S_0 hem). **b** Detail of the S_0 hematite shown in **a**, where fluid inclusions tend to cluster in the core (*arrow*). Note that the margins are devoid of fluid inclusions. **c** An early S_1-overprinting hematite can be distinguished by poorly elongated crystals without obvious preferential arrangement of fluid inclusions (*arrows*). **d** A late S_1-overprinting hematite is characterised by well elongated laths with cleavage-controlled arrays of fluid inclusions (*arrows*)

liquid-only fluid inclusions suggest formation temperatures of less than 200°C (cf. Samson and Banks 1988). Numerous fluid inclusions are empty or decrepitated.

Boron-isotope composition of tourmaline

Selected tourmaline crystals dispersed in the talcose matrix were analysed for $^{11}B/^{10}B$ ratios on one polished thin section. The tourmaline crystals attain up to ~150 μm in length, and their $\delta^{11}B$ values are remarkably negative, varying from −20‰ to −12‰ (Table 7 ESM, Fig. 11). No clear isotopic zoning was observed.

Discussion

A summary of the hematite and talc fabrics and their geological scenario is sketched in Fig. 12. The strong positive linear correlation between total Fe and S (Fig. 9b) may be an analytical artefact due to influence of the high-Fe matrix effect from hematite-rich rocks on the quantitative determination of S. However, total Fe and S contents from itabirite and soft hematite, determined by the same methods, do not plot along the linear distribution. This effectively rules out any high-Fe matrix effect. The acid digestion ICP technique employed is considered to yield sulfide S because sulfate S associated with barite cannot be dissolved. Since sulfide minerals have not been found in the hematite–talc schist, it may be assumed that the whole-rock S values reflect sulfate S from fluid inclusions hosted in tabular hematite. The trace amounts of S detected by electron-microprobe analyses of tabular hematite (Table 4 ESM), particularly the S_1-overprinting hematite, may result from the abundant fluid inclusions (Fig. 10). Direct evidence for high amounts of sulfate dissolved in hematite-hosted fluid inclusions comes from crush-leach analyses of S_1-overprinting hematite from several localities in the Quadrilátero Ferrífero (Lüders et al. 2005). It is thus suggested that the whole-rock S values represent sulfate S from hematite-trapped fluid inclusions.

The Gongo Soco talc mineralisation and its soft hematite ore seem to have had a common protolith as based on field and petrographical observations. They share similar tectonic fabrics and the S_1-overprinting hematite. Talc is an accessory component of the soft hematite ore, where it occurs as dispersed aggregates. In the fresh wall-rock itabirite, dolomite was partially replaced by talc (Fig. 4b). In the open cast, dolomite pods have recently been exposed within the hematite–talc schist. These observations suggest the replacement of dolomite by talc. Dolomitic itabirite is, therefore, the most likely candidate for the protolith of both the talc mineralisation and the soft hematite ore. Ductile deformation, facilitated by talc, would have produced in the .talcose schist the penetrative tectonic fabric of S_1 hematite

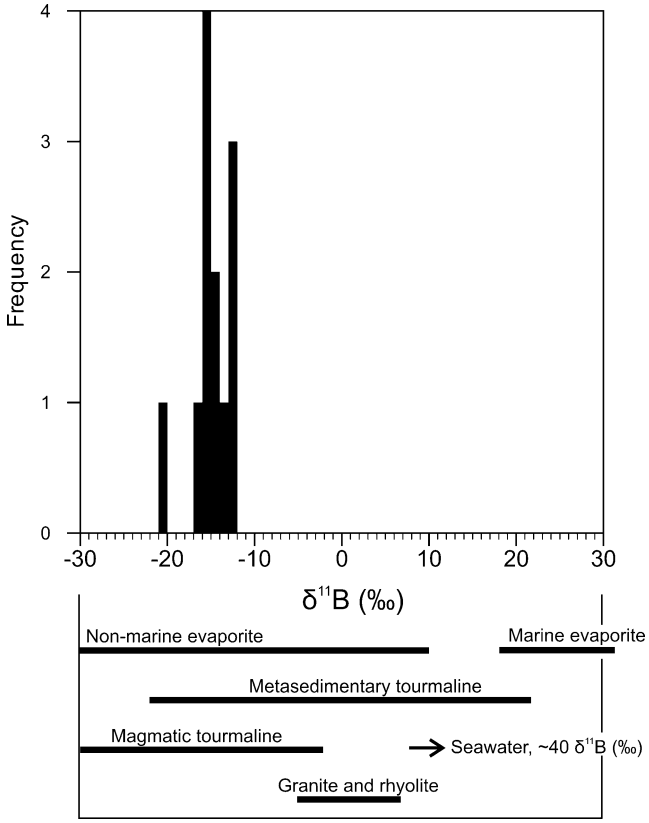

Fig. 11 Histogram of tourmaline $\delta^{11}B$ values (Table 7 ESM) for hematite–talc schist, Gongo Soco, and variation of $\delta^{11}B$ in some reservoirs (Barth 1993). The tourmaline composition (Fig. 8) and its range of negative $\delta^{11}B$ values, together with the abundance of F-bearing talc at Gongo Soco, favour a non-marine evaporitic reservoir for the talc-mineralising fluid system (vide Discussion)

that has been found in the soft hematite ore. As oxidation conditions were buffered by hematite, talc was favoured instead of minnesotaite.

The replacement of dolomite and ankerite by talc would release Mn (Table 1 ESM). The released Mn best explains the relatively high contents of Mn in portions of the soft hematite ore and hematite–talc schist. Because of the hematite-buffered environment, oxidation conditions were not high enough for the co-precipitation of tetravalent Mn oxides and hematite. Any tetravalent Mn oxide necessarily post-dates hematite, filling the interstices of the S_1-overprinting hematite (Fig. 7a). The interstitial manganiferous material (Fig. 7b) is carbonaceous and Cl-bearing (Fig. 7d). Chlorine is confirmed in the whole-rock chemistry, i.e. 1.3 wt% Cl, in the sample with the highest Mn content, i.e. 3.5 wt% Mn (Table 6). The formation of carbonaceous wad after ankerite breakdown can be represented as follows:

$$2Mn^{2+} + HCO_3^- + H_2O = 2MnO_2 + C + 3H^+$$

This reaction is the inorganic Mn-oxidising analogue of the organically mediated reduction of Mn dioxide that is

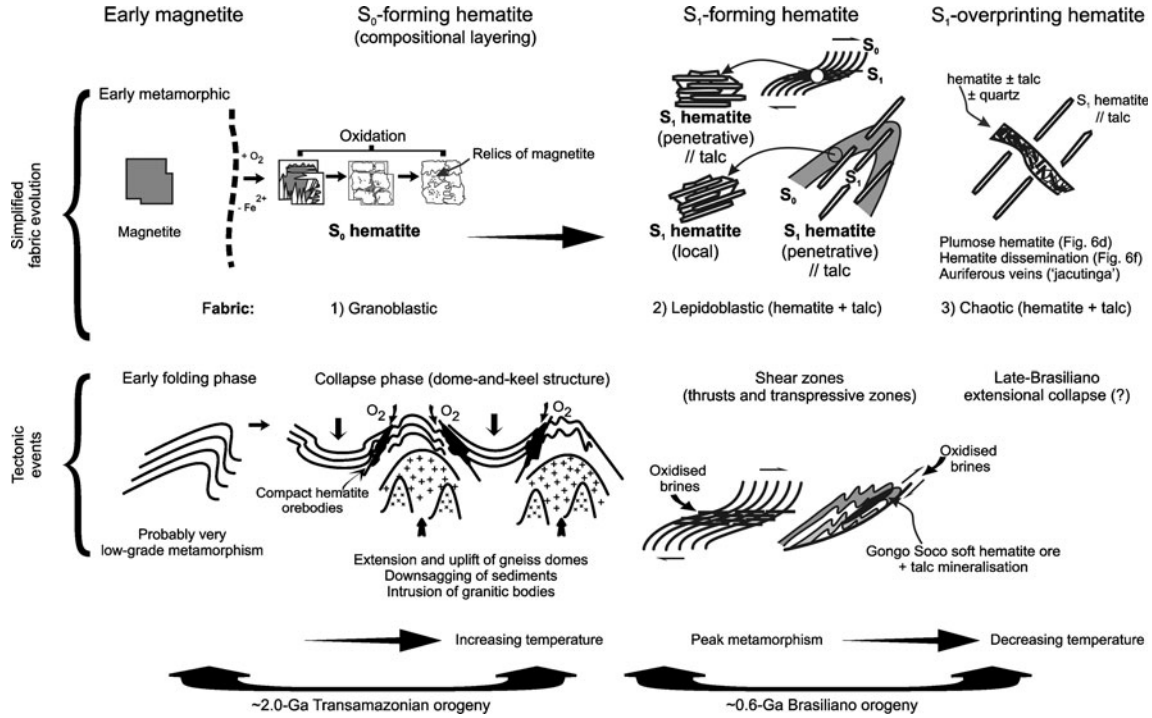

Fig. 12 Schematic model for the evolution of different types of hematite and associated talc, in relation to the tectonic fabrics observed at Gongo Soco. The model has been simplified and adapted from Rosière and Rios (2004). The earliest recognisable hematite occurs as granoblastic hematite after magnetite, i.e. martite, defining the compositional layering (S_0) of itabiritic rocks. This S_0 hematite is mostly preserved in the western part of the Quadrilátero Ferrífero. In those parts affected by the ~0.6 Brasiliano tectonics, i.e. in its central and eastern parts, the S_0 hematite is obliterated by tabular hematite (S_1 hematite) in shear zones and fold hinges. The S_1-hematite fabrics form the penetrative tectonic foliation that characterises the Brasiliano-overprinted parts of the Quadrilátero Ferrífero. These tectonic hematite fabrics are cross-cut by veins and pockets, which contain hematite and talc without preferred orientation. This chaotic hematite, i.e. here referred to as S_1-overprinting hematite, is also disseminated in the Gongo Soco soft hematite ore and in contact zones between the soft hematite ore and hematite–talc schist

widely described in groundwater systems (e.g. Freeze and Cherry 1979).

The infrared fluid-inclusion petrography suggests formation temperatures of less than 200°C for the S_1-overprinting hematite in the hematite–talc schist. This estimate matches the microthermometric data of about 160°C for the S_1-overprinting hematite from Au–Pd-bearing veins (Lüders et al. 2005). A maximum temperature estimate of ~300°C (Table 2 ESM) can be obtained from the S_1-overprinting chlorite (Fig. 7a, c). The temperatures were calculated using the equation of Kranidiotis and MacLean (1987) and assuming that no ferric Fe replaces Al in tetrahedral sites. As a consequence of this assumption, charge balance implies that most Fe, if not all, is ferric. Although caution is needed, reporting all chlorite Fe as Fe_2O_3 gives totals close to 100%, in line with the highly oxidised, hematite-rich rocks.

The tourmaline composition from sparsely disseminated crystals within the hematite–talc schist follows the povondraite–"oxy-dravite" trend (Fig. 8). This compositional trend is considered diagnostic of meta-evaporitic tourmaline, which formed from oxidising and highly saline fluids (Henry et al. 2008). Such a meta-evaporitic fluid origin finds support in the presence of abundant F-bearing talc (cf. Cook and Ashley 1992; Garnier et al. 2004) and in the halogen ratios of fluid inclusions in quartz and S_1-overprinting hematite from hematitic veins (Lüders et al. 2005). Also, Ti in hematite, with some hundreds micrograms per gram to a few wt% Ti (Table 4 ESM; and Cabral et al. 2003, 2006), implies highly saline fluids because the solubility of rutile dramatically increases in F-rich brines (Rapp et al. 2010).

These pieces of evidence, however, do not distinguish between marine and non-marine evaporitic fluids. In this regard, B-isotope ratios in tourmaline are a powerful tool for constraining the B source. Taking into account formational temperatures in the range of 200°C to 300°C for the Gongo Soco tourmaline and experimental B-isotope fractionation (Meyer et al. 2008; c.f. Palmer et al. 1992 for different fractionation equations), the tourmaline $\delta^{11}B$ values (Table 7 ESM, Fig. 11) would require hydrothermal fluids with $\delta^{11}B$ values between −16‰ and −7‰. This compositional range excludes a marine evaporitic origin, implying a non-marine evaporitic reservoir for B (Palmer and Slack 1989; Slack et al. 1993). A magmatic reservoir

for B would also be compatible with the $\delta^{11}B$ range. Although magmatic B cannot be ruled out based on the tourmaline $\delta^{11}B$ values, a magmatic fluid source is less likely to have had any substantial contribution to the hydrothermal fluid system. One reason is the absence of Brasiliano plutonic rocks in the Quadrilátero Ferrífero. Another reason is the abundance of sulfate in quartz- and hematite-hosted fluid inclusions from S_1-truncating veins (Lüders et al. 2005). High contents of aqueous sulfate are commonly found in fluids that dissolved evaporitic gypsum. In summary, the tourmaline chemistry, the F-bearing talc, the titaniferous hematite at Gongo Soco and available data from the literature (Lüders et al. 2005) are consistent with oxidised brines of non-marine evaporitic origin.

Studies indicating a non-marine evaporitic environment within the Palaeoproterozoic Itabira Group are, nevertheless, lacking. Spier et al. (2007) argued that dolomitic itabirite precipitated in shallow marine waters with some terrigenous component; no evaporitic environment was proposed. On the other hand, recent diamond drilling supervised by one of us (A. A. Seabra Gomes Jr.) has revealed halite as disseminations in dolomite of the Gandarela Formation in the Gongo Soco property. Interestingly, barite mineralisation occurs as veins truncating the Brasiliano tectonic foliation in dolomitic rocks of the Gandarela Formation nearby Ouro Preto (von Freyberg 1934; Lacourt 1938; A.R. Cabral, unpublished field observations). Tourmaline is locally abundant as tourmalinite in the Batatal Formation (e.g. Cavalcanti and Xavier 2006; Vial et al. 2007). Some B-isotope data have been reported from the Batatal Formation at the Passagem de Mariana gold deposit. There, gold mineralisation occurs as tourmaline-rich quartz veins (Vial et al. 2007, and references therein), in which tourmaline has SIMS $\delta^{11}B$ values between −19‰ and −12‰ (Garda et al. 2010). This range of tourmaline $\delta^{11}B$ values coincides with that from the Gongo Soco talc mineralisation (Table 7 ESM, Fig. 11). Here, we reinterpret Garda et al.' $\delta^{11}B$ data for Passagem: the abundance of tourmaline and its negative $\delta^{11}B$ values suggest a non-marine evaporitic reservoir, where concentrations of borate minerals are typical (e.g. Slack et al. 1993; Warren 2006).

Conclusion

Shear zone-channelled hydrothermal fluid leached gangue minerals from dolomitic itabirite, converting it to soft hematite ore and hematite–talc schist enriched in F. Talc is the major repository of F. The fluid system was very oxidising and evolved from strain-induced, foliation-forming tabular hematite, to strain-free, chaotically oriented tabular hematite. The presence of F in talc and Ti in hematite points to Ti mobilisation by F-rich brines. Tourmaline from the talc mineralisation has chemical compositions that are diagnostic of meta-evaporitic tourmaline. The tourmaline B-isotope signature is compatible with a non-marine evaporitic reservoir. The breakdown of dolomite and ankerite from dolomitic itabirite released C and some Mn. At higher oxidising conditions, Mn precipitated from Cl-rich fluids as Cl-bearing carbonaceous wad in the interstices of chaotically oriented tabular hematite.

In conclusion, this work presents evidence for an evaporitic fluid source, which most likely accounts for highly saline and oxidising fluids. Such fluids are required to explain the pervasive hematitisation and, notably, the solubility of otherwise immobile Ti to form Ti-bearing hematite. The nature of the evaporitic source is constrained as non-marine by the B-isotope signature of the Gongo Soco tourmaline. Although tourmaline contents are trifling at Gongo Soco, epigenetic tourmaline is locally abundant in metasedimentary rocks of the Minas Supergroup below and above the Itabira Group where affected by the Brasiliano tectonic overprint. It is thus reasonable to propose that the hydrothermal overprint caused by oxidising, non-marine evaporitic brines is not restricted to Gongo Soco, and should be recognised in other metasedimentary rocks along the Brasiliano thrust front (see Cabral et al. 2011).

Acknowledgements We gratefully acknowledge numerous visits to the Gongo Soco mine, initially under Mineração Socoimex, now operated by Companhia Vale do Rio Doce (VALE). Vagner Costa and Douglas José de Oliveira (VALE) are particularly thanked for logistical support and access to internal files. ARC expresses his gratitude to Prof. G. Beaudoin and Prof. B. Lehmann for access to the electron-microprobe facility at Université Laval and TU Clausthal, respectively. Reviews by two anonymous referees, as well as comments by Nikola Koglin, have greatly improved the manuscript.

References

Alkmim FF, Marshak S (1998) Transamazonian orogeny in the southern São Francisco craton region, Minas Gerais, Brazil: evidence for Paleoproterozoic collision and collapse in the Quadrilátero Ferrífero. Precambr Res 90:29–58

Babinski M, Chemale F Jr, Van Schmus WR (1995) The Pb/Pb age of the Minas Supergroup carbonate rocks, Quadrilátero Ferrífero, Brazil. Precambr Res 72:235–245

Barth S (1993) Boron isotope variations in nature: a synthesis. Geol Rund 82:640–651

Cabral AR (2006) Palladiferous Gold Mineralisation (*ouro preto*) in Brazil: Gongo Soco, Itabira and Serra Pelada. Geologisches Jahrbuch, Sonderhefte Reihe D, Heft 8. E. Schweizerbart'sche Science Publishers, Stuttgart, p 115

Cabral AR, Rocha Filho OG, Jones RD (2003) Hydrothermal origin of soft hematite ore in the Quadrilátero Ferrífero of Minas Gerais,

Brazil: petrographic evidence from the Gongo Soco iron ore deposit. Appl Earth Sci (Trans Inst Min Metall Sect B) 112: B279–B286

Cabral AR, Lehmann B, Galbiatti HF, Rocha Filho OG (2006) Evidence for metre-scale variations in hematite composition within the Palaeoproterozoic Itabira Iron Formation, Minas Gerais, Brazil. Mineral Mag 70:591–602

Cabral AR, Lehmann B, Tupinambá M, Schlosser S, Kwitko-Ribeiro R, de Abreu FR (2009) The platiniferous Au–Pd belt of Minas Gerais, Brazil, and genesis of its botryoidal Pt–Pd–Hg aggregates. Econ Geol 104:1265–1276

Cabral AR, Lehmann B, Tupinambá M, Wiedenbeck M, Brauns M (2011) Geology, mineral chemistry and tourmaline B isotopes of the Córrego Bom Sucesso area, southern Serra do Espinhaço, Minas Gerais, Brazil: implications for Au–Pd–Pt exploration in quartzitic terrain. J Geochem Expl. doi:10.1016/j.gexplo.2011.06.007

Cavalcanti JAD, Xavier RP (2006) Origem dos turmalinitos auríferos da região sudeste do Quadrilátero Ferrífero-MG: geologia, petrografia, química mineral e isótopos de Nd. Rev Bras Geociênc 36:646–647

Cook NDJ, Ashley PM (1992) Meta-evaporite sequence, exhalative chemical sediments and associated rocks in the Proterozoic Willyama Supergroup, South Australia: implications for metallogenesis. Precambr Res 56:211–226

Dalstra H, Guedes S (2004) Giant hydrothermal hematite deposits with Mg–Fe metasomatism: a comparison of the Carajás, Hamersley, and other iron ores. Econ Geol 99:1793–1800

Dorr JVN (1964) Supergene iron ores of Minas Gerais, Brazil. Econ Geol 59:1203–1240

Dorr JVN (1969) Physiographic, stratigraphic and structural development of the Quadrilátero Ferrífero, Minas Gerais, Brazil. US Geol Surv Prof Pap 641-A

Dyar MD, Wiedenbeck M, Robertson D, Cross LR, Delaney JS, Ferguson K, Francis CA, Grew ES, Guidotti CV, Hervig RL, Hughes JM, Husler J, Leeman W, McGuire AV, Rhede D, Rothe H, Paul RL, Richards I, Yates M (2001) Reference minerals for microanalysis of light elements. Geostandards Newsletter 25:441–463

Eichler J (1967) Das physikalisch-chemische Milieu bei der Verwitterung von Itabiriten in Minas Gerais/Brasilien. Chem Erde 26:119–132

Freeze RA, Cherry JA (1979) Groundwater. Prentice-Hall, Englewood Cliffs, p 604

von Freyberg B (1934) Die Bodenschätze des Staates Minas Geraes (Brasilien). E. Schweizerbart'sche Verlagsbuchhandlung, Stuttgart, p 453

Garda GM, Xavier RP, Cavalcanti JAD, Trumbull RB, Wiedenbeck M (2010) Significance of compositional and boron isotope variations in tourmaline of Passagem de Mariana gold mine, Quadrilátero Ferrífero, Minas Gerais, Brazil. Acta Mineral-Petrogr Abst Ser 6:483

Garnier V, Ohnenstetter D, Giuliani G (2004) L'aspidolite fluorée: rôle des évaporites dans la genèse du rubis des marbres de Nangimali (Azad-Kashmir, Pakistan). C R Geosci 336:1245–1253

Gonfiantini R, Tonarini S, Gröning M, Adorni-Braccesi A, Al-Ammar AS, Astner M, Bächler S, Barnes RM, Bassett RL, Cocherie A, Deyhle A, Dini A, Ferrara G, Gaillardet J, Grimm J, Guerrot C, Krähenbühl U, Layne G, Lemarchand D, Meixner A, Northington DJ, Pennisi M, Reitznerová E, Rodushkin I, Sugiura N, Surberg R, Tonn S, Wiedenbeck M, Wunderli S, Xiao Y, Zack T (2003) Intercomparison of boron isotope and concentration measurements. Part II: evaluation of results Geostandards Newsletter 27:41–57

Guimarães D (1953) Notas à margem da crítica. Instituto de Tecnologia Industrial, Estado de Minas Gerais, Belo Horizonte, Avulso 16

Harder EC, Chamberlin RT (1915) The geology of central Minas Gerais, Brazil. J Geol 23:341–378, 385–424

Hartmann LA, Endo I, Suita MTF, Santos JOS, Frantz JC, Carneiro MA, McNaughton NJ, Barley ME (2006) Provenance and age delimitation of Quadrilátero Ferrífero sandstones based on zircon U–Pb isotopes. J South Am Earth Sci 20:273–285

Henry DJ, Sun H, Slack JF, Dutrow BL (2008) Tourmaline in metaevaporites and highly magnesian rocks: perspectives from Namibian tourmalinites. Eur J Mineral 20:889–904

Henwood WJ (1871) On the gold mines of Minas Geraes, in Brazil. Trans R Geol Soc Cornwall 8:168–370

Herz N (1978) Metamorphic rocks of the Quadrilátero Ferrífero, Minas Gerais, Brazil. US Geol Surv Prof Pap 641-C

Hippertt J, Davis B (2000) Dome emplacement and formation of kilometre-scale synclines in a granite–greenstone terrain (Quadrilátero Ferrífero, southeastern Brazil). Precambr Res 102:99–121

Koglin N, Frimmel HE, Minter WEL, Brätz H (2010) Trace-element characteristics of different pyrite types in Mesoarchaean to Palaeoproterozoic placer deposits. Miner Deposita 45:259–280

Kranidiotis P, MacLean WH (1987) Systematics of chlorite alteration at the Phelps Dodge massive sulfide deposit, Matagami, Quebec. Econ Geol 82:1898–1911

Lacourt F (1938) Baritita e pirita no município de Ouro Preto, Minas Gerais. Mineração e Metallurgia 3:298–301

Leeman WP, Tonarini S (2001) Boron isotopic analyses of proposed borosilicate mineral reference samples. Geostandards Newsletter 25:399–403

Lima TAF, Rios FJ, Meireles HP, Yardley B (2009) Fe-ore forming fluids in the Espinhaço Supergroup, Minas Gerais, Brazil. In: Williams PJ (ed) Smart science for exploration and mining. James Cook University, Townsville, Australia, pp 564–566

Lüders V, Romer RL, Cabral AR, Schmidt C, Banks DA, Schneider J (2005) Genesis of itabirite-hosted Au–Pd–Pt-bearing hematite-(quartz) veins, Quadrilátero Ferrífero, Minas Gerais, Brazil: constraints from fluid inclusion infrared microthermometry, bulk crush-leach analysis and U–Pb systematics. Miner Deposita 40:289–306

Meyer C, Wunder B, Meixner A, Romer RL, Heinrich W (2008) Boron-isotope fractionation between tourmaline and fluid: an experimental re-investigation. Contrib Mineral Petrol 156:259–267

Noce CM (2000) Geochronology of the Quadrilátero Ferrífero: a review. Geonomos 8:15–23

Palmer MR, Slack JF (1989) Boron isotopic composition of tourmaline from massive sulfide deposits and tourmalinites. Contrib Mineral Petrol 103:434–451

Palmer MR, London D, Morgan VIGB, Babb HA (1992) Experimental determination of fractionation of $^{11}B/^{10}B$ between tourmaline and aqueous vapor: a temperature- and pressure-dependent isotopic system. Chem Geol 101:123–129

Pires FRM (1995) Textural and mineralogical variations during metamorphism of the Proterozoic Itabira Iron Formation in the Quadrilátero Ferrífero, Minas Gerais, Brazil. An Acad Bras Ci 67:77–105

Rapp JF, Klemme S, Butler IB, Harley SL (2010) Extremely high solubility of rutile in chloride and fluoride-bearing metamorphic fluids: an experimental investigation. Geol 38:323–326

Rosière CA, Rios FJ (2004) The origin of hematite in high-grade iron ores based on infrared microscopy and fluid inclusion studies: the example of the Conceição mine, Quadrilátero Ferrífero, Brazil. Econ Geol 99:611–624

Rosière CA, Rios FJ (2006) Specularitic iron ores and shear zones in the Quadrilátero Ferrífero District. Appl Earth Sci (Trans Inst Min Metal B) 115:B134–B138

Rosière CA, Spier CA, Rios FJ, Suckau VE (2008) The itabirites of the Quadrilátero Ferrífero and related high-grade iron ore deposits: an overview. Rev Econ Geol 15:223–254

Samson IM, Banks DA (1988) Epithermal base-metal vein mineralization in the Southern Uplands of Scotland: nature and origin of the fluids. Miner Deposita 23:1–8

Slack JF, Palmer MR, Stevens BPJ, Barnes RG (1993) Origin and significance of tourmaline-rich rocks in the Broken Hill district, Australia. Econ Geol 88:505–541

Spier CA, de Oliveira SMB, Rosière CA (2003) Geology and geochemistry of the Águas Claras and Pico iron mines, Quadrilátero Ferrífero, Minas Gerais, Brazil. Miner Deposita 38:751–774

Spier CA, de Oliveira SMB, Sial AN, Rios FJ (2007) Geochemistry and genesis of the banded iron formations of the Cauê Formation, Quadrilátero Ferrífero, Minas Gerais, Brazil. Precambr Res 152:170–206

Tonarini S, Pennisi M, Adorni-Braccesi A, Dini A, Ferrara G, Gonfiantini R, Wiedenbeck M, Gröning M (2003) Intercomparison of boron isotope concentration measurements. Part I: Selection, preparation and homogeneity tests of the intercomparison materials. Geostandards Newsletter 27:21–39

Vial DS, Duarte BP, Fuzikawa K, Vieira MBH (2007) An epigenetic origin for the Passagem de Mariana gold deposit, Quadrilátero Ferrífero, Minas Gerais, Brazil. Ore Geol Rev 32:596–613

Warren JK (2006) Evaporites: Sediments, Resources and Hydrocarbons. Springer, Berlin, p 1035

Wiedenbeck M, Rhede D, Lieckefett R, Witzki H (2004) Cryogenic SIMS and its applications in the earth sciences. Appl Surf Sci 231–232:888–892